

Excimer Luminescence From Nonresonantly Excited Pyrene and Perylene Molecules in Solution

Kazuya Nakagawa,[†] Yudai Numata,[†] Heisuke Ishino,[†] Daichi Tanaka,[†] Takayoshi Kobayashi,[‡] and Eiji Tokunaga^{*,†,§}

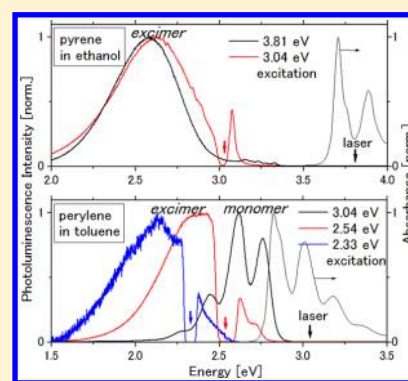
[†]Department of Physics, Faculty of Science, Tokyo University of Science, 1-3 Kagurazaka, Shinjuku-ku, Tokyo 162-8601, Japan

[‡]Advanced Ultrafast Laser Research Center, University of Electro-Communications, 1-5-1 Chofugaoka, Chofu, Tokyo 182-8585 Japan

[§]Research Center for Green and Safety Sciences, Tokyo University of Science, 1-3 Kagurazaka, Shinjuku-ku, Tokyo 162-8601, Japan

S Supporting Information

ABSTRACT: By nonresonant excitation below the absorption edge of pyrene and perylene molecules in solution, efficient excimer luminescence is observed. For perylene in solution, there are two kinds of nonresonant excimer emission that closely resemble Y- and E-emissions in perylene crystal and perylene in polymer. The concentration dependence of the photon flux density of monomer and excimer emission is reasonably explained by a simple model with a few fitting parameters based on the ordinary excimer formation process, in which the excited-state monomer interacts with a ground-state monomer. Observed quantum efficiency of excimer formation is by orders of magnitude higher than that expected if a monomer is excited from thermally populated vibrational levels. The experimental evidence for direct resonant excitation of excimers in perylene nanocrystals is obtained from the absence of anti-Stokes emission. This is due to a symmetry-breaking effect close to crystal surface, suggesting that excimers are formed through a more efficient process in solution, such as resonant excitation of weakly interacting molecules with a symmetry-broken intermolecular configuration.



I. INTRODUCTION

Pyrene and perylene are prototypical polycyclic conjugated hydrocarbons. Both crystals have a dimeric structure,¹ so that photoexcited states yields a characteristic excimer emission. It is also called self-trapped exciton in terms of the exciton in crystal.² On resonant excitation of these molecules in solution, it is well-known that excimer luminescence is readily observed for pyrene at high concentration.^{3–5} By contrast, it is difficult to observe excimer luminescence for perylene in solution even at saturated concentration.^{6,7}

The reason for this difference could be attributed to difference in lifetime of the excited state of monomer molecules. Since the lifetime of the lowest singlet excited state of pyrene is 440 ns (cyclohexane solution) or 290 ns (ethanol solution)^{3,4} while that of perylene is 5.8 ns (toluene solution),⁷ chiefly reflecting the oscillator strength of radiative transition. The excited pyrene molecules are accumulated by photoexcitation during the long lifetime to increase chance to collide with a ground-state molecule to make an excited dimer, i.e., excimer. On the other hand, the excited perylene molecules have a much shorter lifetime ($\sim 1/100$), so it is difficult for them to accumulate to a high concentration. Therefore, excimer emission spectra in perylene solution have been obtained as difference spectra between photoluminescence spectra of different concentrations^{6,7} or on limited conditions such as under high pressure.⁸

In this paper, we have found that excimer emission can be observed by nonresonant excitation of pyrene and perylene molecules in solution. In addition, two types of excimer emissions (E and Y), which are usually observed in crystals,^{9,10} are observed by nonresonant excitation of perylene solution. There is an increased interest in nonresonant excitation effects in microcrystals and nanoscopic structures.^{11,12} There has been, however, little systematic investigation about nonresonant excitation effects on molecules. For comparison, the effect on perylene nanocrystals is also examined to find evidence for resonant excitation process of excimers.

II. EXPERIMENTAL SECTION

Pyrene (>99%) and perylene (>98%) (TCl, Tokyo Chemical Industry) were purified by sublimation, once for pyrene and twice for perylene. For solution samples, ethanol (>99.5%, Wako) and toluene (>99.8%, Wako) were used as solvent without further purification (Solution was not deoxygenated). For the effect of dissolved oxygen, see Supporting Information). For polymer samples, polymethyl methacrylate (PMMA) and perylene were dissolved in chloroform and the solution was cast on a coverslip. The perylene concentration of the polymer films were measured as x mol %, perylene x mol against MMA

Received: March 7, 2013

Revised: October 14, 2013

Published: October 14, 2013

100 mol (monomeric unit $C_5H_8O_2$). Bulk α -perylene crystals were grown from gas phase by sublimation, and nanocrystals of α -perylene were made with the reprecipitation method.^{13,14} Steady-state absorption measurements were carried out with an absorption spectrophotometer (Shimadzu, UV-3150). All the experiments were performed at room temperature unless specifically noted. For photoexcitation of samples, continuous wave (cw) lasers were used as follows: a HeCd laser for 325 nm, a laser diode for 408 nm, an Ar ion laser for 488 nm, and a diode-laser pumped solid-state laser for 532 nm. They were irradiated on a sample without focus at the intensity from 5.8 mW/cm^2 (resonant excitation) to 8500 mW/cm^2 (nonresonant excitation). Since nonresonant emission intensity is extremely small, monochromatic light from an incoherent light source could not be used. A 30-cm spectrometer (Acton) with a liquid-nitrogen cooled charge-coupled device (CCD; Roper Scientific) was used for acquisition of emission spectra. Scattering of the excitation laser light was blocked with an appropriate notch filter.

III. RESULTS

Figure 1 shows the absorption spectra of pyrene in ethanol¹⁵ and of perylene in toluene, and photoluminescence (PL)

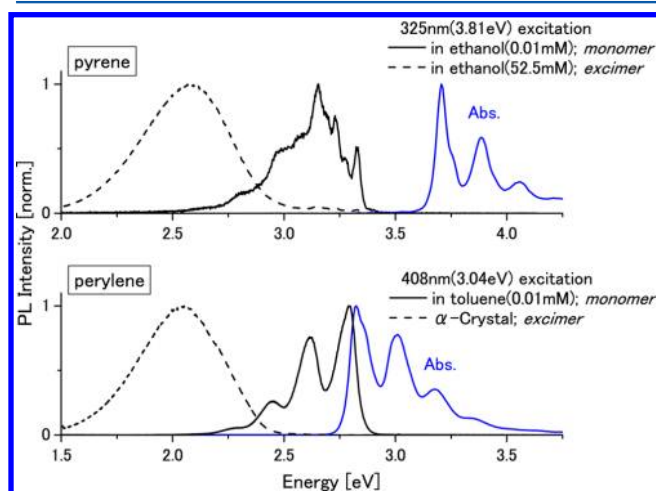


Figure 1. Absorption and PL spectra of pyrene in ethanol and perylene in toluene. For pyrene, monomer emission at 0.01 mM and excimer emission at 52.5 mM (saturated concentration) at 325 nm (3.81 eV) resonant excitation. For perylene, monomer emission at 0.01 mM and excimer emission in a bulk α -crystal at 408 nm (3.04 eV) resonant excitation.

spectra of them on resonant excitation both at low-concentration and nearly saturated solutions. Pyrene solution shows excimer emission,^{3,16} while perylene solution does not even at the saturated concentration.^{6–8} The lowest excited state in pyrene is the 1L_b state,¹⁷ which is a dipole-transition forbidden state. The oscillator strength is as low as $\sim 10^{-2}$ (partially allowed by vibronic coupling), which is why the monomer excited state has a longer lifetime. In Figure 1, the corresponding absorption is not seen below the detection limit, but emission occurs from this state.

Figures 2 and 3 show PL spectra of pyrene and perylene, respectively, on nonresonant excitation. It is evident that excimer-like emissions are observed not only in pyrene solution but also in perylene solution. In Figure 4, nonresonant emission spectra of perylene solution in Figure 3 are compared with

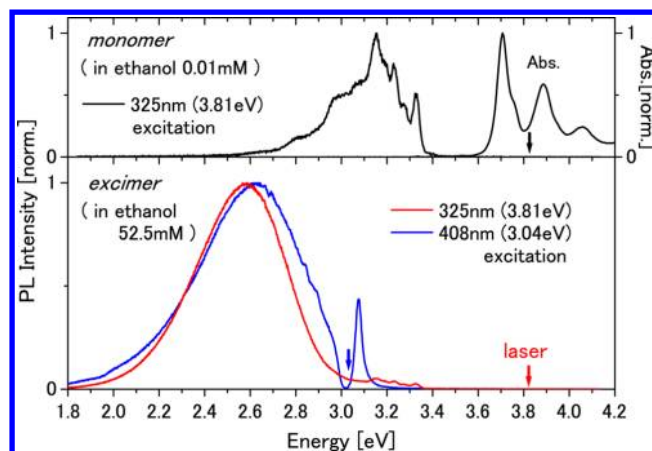


Figure 2. Excimer emission spectra of pyrene in saturated ethanol solution by resonant (325 nm = 3.81 eV, 17 mW/cm^2 , black line) and nonresonant (408 nm = 3.04 eV, 8500 mW/cm^2 , red line) excitation, compared with absorption and emission spectra of monomers above.

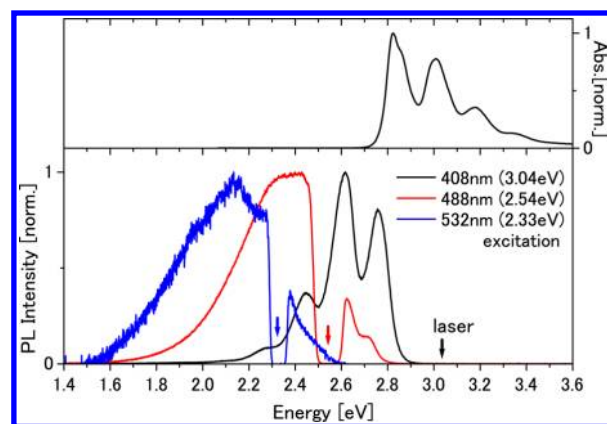


Figure 3. Excimer emission spectra of perylene in saturated toluene solution (10 mM) by resonant (408 nm = 3.04 eV, 5.8 mW/cm^2 , black line) and nonresonant (488 nm = 2.54 eV, 37 mW/cm^2 , red line, and 532 nm = 2.33 eV, 260 mW/cm^2 , blue line) excitation, compared with the absorption spectrum of monomers above.

those of bulk α -perylene crystal, perylene nanocrystals, and perylene molecules dispersed in a polymer (PMMA) film.^{18,19} In polymer film, the concentration of molecules can be adjusted to values between for crystal and for solution. The details of the experimental results for polymer are shown in Figure 5. For the PMMA film with less than or equal to 1.5 mol % concentration of perylene, molecules are apparently homogeneously dispersed while that with 5.0 mol % concentration shows an inhomogeneous distribution, suggesting crystal formation. In fact, the extinction spectra show the monomer absorption for 0.1, 0.5, and 1.0 mol % films, while the films at 3.0 and 5.0 mol % show exciton absorption or crystal absorption (see Supporting Information). It can be found from Figures 3 to 5 that there are two-types of excimer emission for perylene, i.e., Y- and E-emission besides monomer emission. In bulk α -perylene crystal, E-emission is observed above 50 K while Y-emission is observed below 50 K.^{9,20} E-emission is from dimers of the nearest neighbor pair, while Y-emission is assigned to dimers of the second nearest parallel pair in the α -crystal.¹⁰ It is interesting to note that not only E-emission but also Y-emission tends to prevail even in polymer¹⁹ and in solution. To the best

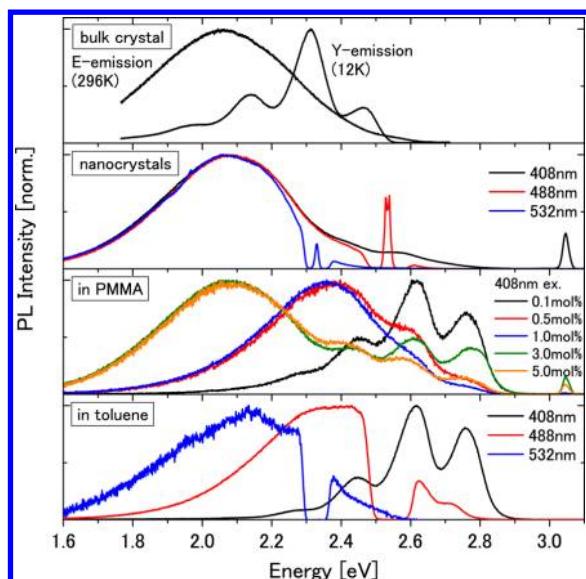


Figure 4. Resonant (408 nm, 3.04 eV) and nonresonant (488 nm = 2.54 eV, 532 nm = 2.33 eV) emission spectra of perylene nanocrystals of 168 nm average diameter, perylene in polymer (PMMA) at various concentrations, and perylene in toluene, compared with resonant emission spectra in bulk α -crystal at room (296 K) and low (12 K) temperature.

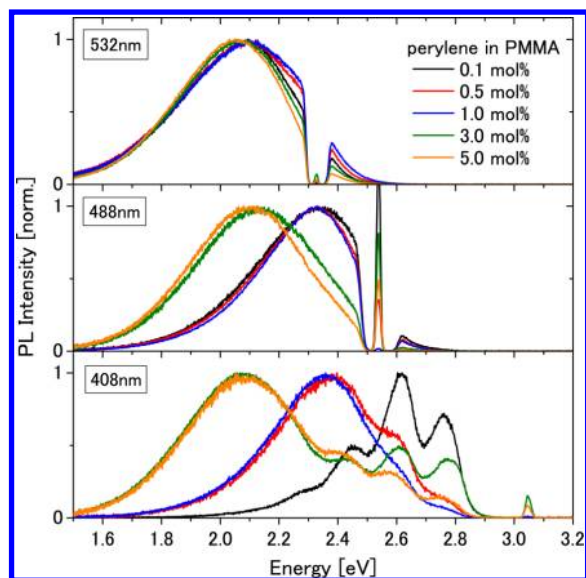


Figure 5. Photoluminescence (PL) spectra of perylene in PMMA from 0.1 mol % to 5.0 mol % on resonant (408 nm = 2.54 eV) and nonresonant (488 nm = 2.54 eV, 532 nm = 2.33 eV) excitation. Here, 1.0 mol % means one perylene molecule per 100 methyl methacrylate monomers. Molecules are homogeneously dispersed in 0.1 mol %, 0.5 mol %, and 1.0 mol % films to show the monomer absorption spectra, while 3.0 mol % and 5.0 mol % films apparently contain inhomogeneity due to crystal formation to show the crystal absorption spectra (Supporting Information).

of our knowledge, Y-emission from perylene in solution is the first observation.

In order to clarify the mechanism of excimer formation by nonresonant excitation, the excitation intensity and the concentration dependence of the excimer emission were studied. As shown in Figure 6, the photoluminescence intensity depends linearly on the nonresonant excitation intensity, so

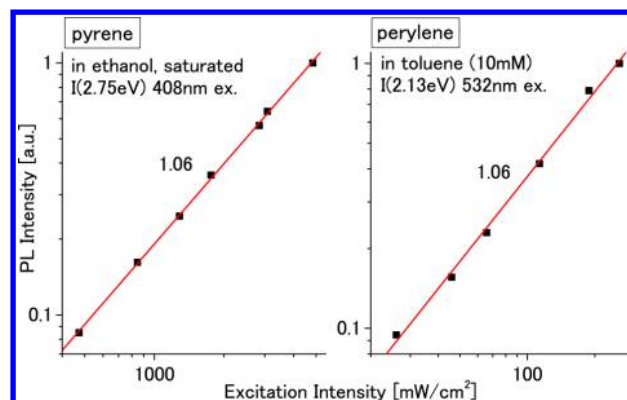


Figure 6. The excitation-intensity dependence of nonresonantly excited excimer emission intensity for pyrene and perylene in solution.

that the excitation mechanism is the one-photon process. Figures 7 and 8 show the concentration (C) dependence of

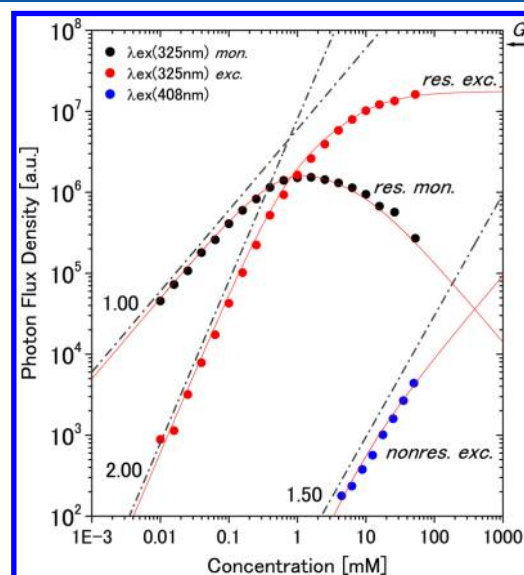


Figure 7. The concentration dependence of emitted photon flux density for pyrene in ethanol. The saturated concentration is ~ 10 mM. Dots are experimental results, and red lines are fitted curves. Resonant monomer (black dots) and excimer (red dots) emission at 325 nm excitation, and nonresonant excimer emission (blue dots) at 408 nm excitation. The dash-dotted lines show the concentration power dependence (C^m) as guides for the eyes. In the fitting, given parameters are $\tau_m = 20$ ns, $\tau_m/\tau_{mr} = 0.030$, $k = 7 \times 10^6$ (mM) $^{-1}$ (s) $^{-1}$, and $a(\lambda_{ex} = 325 \text{ nm}) = 2.55$ (mM) $^{-1}$ (mm) $^{-1}$ while adjusted parameters whose values are determined from the fitting are G_p , $a(\lambda_{ex} = 408 \text{ nm}) = 5.4 \times 10^{-6}$ (mM) $^{-1}$ (mm) $^{-1}$, and $\tau_e/\tau_{er} = 0.26$.

emitted photon flux density in pyrene and perylene solution to compare relative quantum efficiency including excitation efficiency. Here, the emitted photon flux density is normalized by the incident (excitation) photon flux density. Highest care was taken for the collection efficiency of the photoluminescence to be maintained to be the same throughout the whole measurement to minimize experimental error. It was confirmed that no detectable photoluminescence was observed from the solvents (ethanol and toluene).

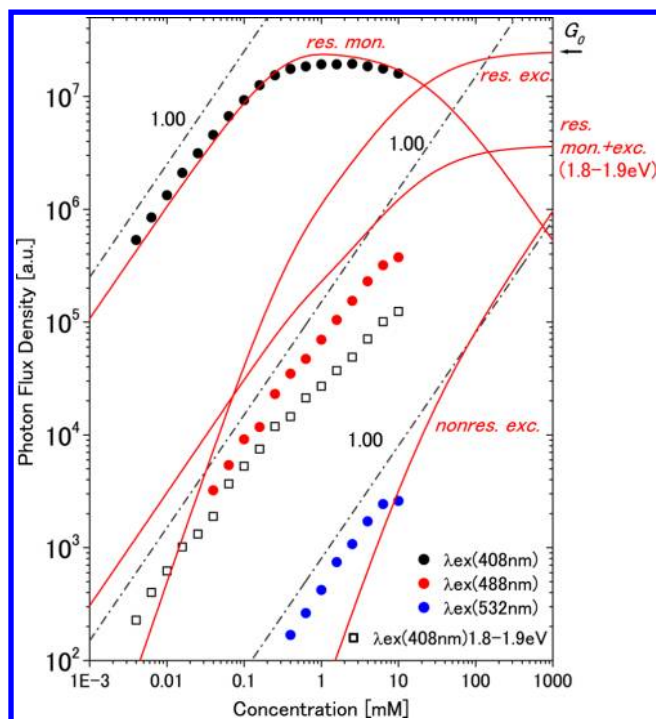


Figure 8. The concentration dependence of emitted photon flux density for perylene in toluene. The saturated concentration is ~ 50 mM. Dots and squares are experimental results, and red lines are fitted curves. The red dots are not fitted with the model because it does not include Y-emission. Resonant monomer (black dots at 408 nm excitation) and nonresonant excimer (red dots at 488 nm and blue dots at 532 nm excitation) emission. Open squares show a part of the photon flux density integrated between 1.8 and 1.9 eV in the spectra, which includes both monomer and excimer emission. The dash-dotted lines are guides for the eyes indicating the linear dependence on the concentration. In the fitting, given parameters are $\tau_m = 5.8$ ns, $k = 8 \times 10^6$ (mM) $^{-1}$ (s) $^{-1}$, $a(\lambda_{ex} = 408 \text{ nm}) = 4.30$ (mM) $^{-1}$ (mm) $^{-1}$, and $P_m = 0.00285$ and $P_e = 0.147$, while adjusted parameters whose values are determined from the fitting are G_0 and $a(\lambda_{ex} = 532 \text{ nm}) = 4.0 \times 10^{-5}$ (mM) $^{-1}$ (mm) $^{-1}$. The quantum yield of radiative transition for both monomer and excimer is assumed to be unity.

IV. ANALYSIS

The wavelength-dependent absorption coefficients for monomer and excimer are given by

$$\alpha(\lambda) = a(\lambda)C \quad (1)$$

$$\beta(\lambda) = b(\lambda)C^2 \quad (2)$$

with C being the concentration of ground-state monomer molecules. With the incident photon flux density $G[s^{-1}m^{-2}]$, the lifetimes of the excited state of the monomer τ_m and the excimer τ_e , the density of excited-state monomers N_m and excimers N_e , and the excimer formation rate k per concentration and per excited-state monomer density, the rate equations read³

$$\frac{dN_m}{dt} = \alpha(\lambda_{ex})G - \frac{N_m}{\tau_m} - kCN_m \quad (3)$$

$$\frac{dN_e}{dt} = \beta(\lambda_{ex})G + kCN_m - \frac{N_e}{\tau_e} \quad (4)$$

The stationary solutions are

$$N_m = \frac{\alpha(\lambda_{ex})G}{\frac{1}{\tau_m} + kC} \quad (5)$$

$$N_e = \tau_e \left[\beta(\lambda_{ex}) + \frac{\alpha(\lambda_{ex})kC}{\frac{1}{\tau_m} + kC} \right] G \quad (6)$$

Then, for the incident photon flux density G_0 at $\lambda = \lambda_{ex}$ the densities of excited monomer molecules and generated excimers N_m and N_e , and the photon flux density G are

$$N_m(x) = \frac{\alpha(\lambda_{ex})G(x)}{\frac{1}{\tau_m} + kC} \quad (7)$$

$$N_e(x) = \tau_e \left[\beta(\lambda_{ex}) + \frac{\alpha(\lambda_{ex})kC}{\frac{1}{\tau_m} + kC} \right] G(x) \quad (8)$$

$$\frac{dG(x)}{dx} = -[\alpha(\lambda_{ex}) + \beta(\lambda_{ex})]G(x) \quad (9)$$

$$G(x) = G_0 e^{-[\alpha(\lambda_{ex}) + \beta(\lambda_{ex})]x} \quad (10)$$

The photon flux densities for observed monomer $I_m(\lambda_{pl})$ and excimer $I_e(\lambda_{pl})$ emission are calculated considering the reabsorption effect in the sample of thickness L and competing nonradiative relaxation processes ($1/\tau_{m,e} = 1/\tau_{m,e,r} + 1/\tau_{m,e,n}$ with $\tau_{m,e,r}$ and $\tau_{m,e,n}$ being radiative and nonradiative lifetimes of monomers and excimers) by

$$\begin{aligned} I_m(\lambda_{pl}, \lambda_{ex}) &= \frac{1}{\tau_{mr}} \int_0^L dx' N_m(x') e^{-[\alpha(\lambda_{pl}) + \beta(\lambda_{pl})]x'} \\ &= \frac{1}{\tau_{mr}} \frac{a(\lambda_{ex})}{\frac{1}{\tau_m} + kC} G_0 \frac{\{1 - e^{-[a(\lambda_{ex}) + a(\lambda_{pl}) + b(\lambda_{ex})C + b(\lambda_{pl})C]CL}\}}{a(\lambda_{ex}) + a(\lambda_{pl}) + b(\lambda_{ex})C + b(\lambda_{pl})C} \end{aligned} \quad (11)$$

and

$$\begin{aligned} I_e(\lambda_{pl}, \lambda_{ex}) &= \frac{1}{\tau_{er}} \int_0^L dx' N_e(x') e^{-[\alpha(\lambda_{pl}) + \beta(\lambda_{pl})]x'} \\ &= \frac{\tau_e}{\tau_{er}} \left[b(\lambda_{ex}) + \frac{a(\lambda_{ex})k}{\frac{1}{\tau_m} + kC} \right] CG_0 \\ &\quad \times \frac{\{1 - e^{-[a(\lambda_{ex}) + a(\lambda_{pl}) + b(\lambda_{ex})C + b(\lambda_{pl})C]CL}\}}{a(\lambda_{ex}) + a(\lambda_{pl}) + b(\lambda_{ex})C + b(\lambda_{pl})C} \end{aligned} \quad (12)$$

On resonant excitation, $a(\lambda_{ex})$ is large, so that the condition of $[a(\lambda_{ex}) + a(\lambda_{pl}) + b(\lambda_{ex})C + b(\lambda_{pl})C]CL \gg 1$ is satisfied except for a low C condition. Then,

$$I_m(\lambda_{pl}, \lambda_{ex}) \cong \frac{\frac{1}{\tau_{mr}} \frac{a(\lambda_{ex})}{\frac{1}{\tau_m} + kC} G_0}{a(\lambda_{ex}) + a(\lambda_{pl}) + b(\lambda_{ex})C + b(\lambda_{pl})C} \quad (13)$$

$$I_e(\lambda_{pl}, \lambda_{ex}) \cong \frac{\frac{\tau_e}{\tau_{er}} \left[b(\lambda_{ex}) + \frac{a(\lambda_{ex})k}{\frac{1}{\tau_m} + kC} \right] CG_0}{a(\lambda_{ex}) + a(\lambda_{pl}) + b(\lambda_{ex})C + b(\lambda_{pl})C} \quad (14)$$

As $C \rightarrow \infty$ (i.e., $1/(\tau_m k) \ll C$ with $b = 0$),

$$I_m(\lambda_{pl}, \lambda_{ex}) \cong \frac{G_0}{\tau_{mr} k C} \quad (15)$$

$$I_e(\lambda_{pl}, \lambda_{ex}) \cong \frac{\tau_e}{\tau_{er}} G_0 \quad (16)$$

On nonresonant excitation, $a(\lambda_{ex})$ is negligibly small, so that the condition of $[a(\lambda_{ex}) + a(\lambda_{pl}) + b(\lambda_{ex})C + b(\lambda_{pl})C]CL \ll 1$ is satisfied. Then,

$$I_m(\lambda_{pl}, \lambda_{ex}) \cong \frac{1}{\tau_{mr}} \frac{a(\lambda_{ex})}{\frac{1}{\tau_m} + kC} CLG_0 \quad (17)$$

$$\rightarrow \frac{a(\lambda_{ex})}{\tau_{mr} k} LG_0 \quad \text{as } C \rightarrow \infty \left(\frac{1}{\tau_m k} \ll C \right) \quad (18)$$

$$I_e(\lambda_{pl}, \lambda_{ex}) \cong \frac{\tau_e}{\tau_{er}} \left[b(\lambda_{ex}) + \frac{a(\lambda_{ex})k}{\frac{1}{\tau_m} + kC} \right] C^2 LG_0 \quad (19)$$

$$\rightarrow \frac{\tau_e}{\tau_{er}} [b(\lambda_{ex})C + a(\lambda_{ex})] CLG_0 \quad \text{as } C \rightarrow \infty \left(\frac{1}{\tau_m k} \ll C \right) \quad (20)$$

The solid curves in Figures 7 and 8 are the results of fitting to the observed photon flux density as a function of the concentration of pyrene solution using the above model equations. If bC is adjusted to the same order of magnitude as $a(\lambda)$, the fit fails so that we set $b = 0$. Thus resonant excitation of excimer, which is represented by bC , is not important in the excimer formation mechanism in solution. The quantum efficiency of the monomer luminescence in the low-concentration limit ($C = 0$) was given by τ_m/τ_{mr} . This was determined from the experimentally observed luminescence decay time $\tau_m = 20$ ns (Supporting Information) and the radiative decaytime $\tau_{mr} = 670$ ns from literature³ for pyrene as $\tau_m/\tau_{mr} = 20/670 = 0.030$. For perylene, the quantum efficiency of luminescence for both monomer and excimer is assumed to be unity. Thus, free fitting parameters for pyrene in Figure 7 are only three, i.e., G_0 , $a(\lambda_{ex})$ in the nonresonant region, and the quantum efficiency of the excimer luminescence τ_e/τ_{er} . For perylene in Figure 8, free fitting parameters are only two, i.e., G_0 and $a(\lambda_{ex})$ in the nonresonant region. The parameter G_0 reflects the geometrical light excitation and collection efficiency in the experimental setup.

For pyrene, using $\tau_m = 20$ ns (from both radiative and nonradiative decay rates) experimentally determined for air-saturated solution (Supporting Information) and $k = 7 \times 10^6$ (mM)⁻¹(s)⁻¹ from literature^{3,4} and $a(\lambda_{ex} = 325 \text{ nm}) = 2.55$ (mM)⁻¹(mm)⁻¹ from the experiment, $a(\lambda_{ex} = 408 \text{ nm})$ and τ_e/τ_{er} are adjusted to obtain $a(\lambda_{ex} = 408 \text{ nm}) = 5.4 \times 10^{-6}$ (mM)⁻¹(mm)⁻¹ and $(\tau_e/\tau_{er}) = 0.26$. Agreement between experiment and simulation is excellent in the whole concentration range, proving that the simulation model is appropriate. On both resonant and nonresonant excitation with these parameters, $I_m \cong I_e$ at $(1/(\tau_m k)) (\tau_{er}/\tau_e) = C$ ($C = 0.82$ mM). For $(1/(\tau_m k)) (\tau_{er}/\tau_e) < C$ on resonant excitation, $I_m < I_e$ to lead to the saturated behavior as in eqs 15 and 16. On nonresonant ($\lambda_{ex} = 408 \text{ nm}$) excitation, $I_m < I_e$ and $I_e \propto C \sim C^2$ for $(1/(\tau_m k)) (\tau_{er}/\tau_e) < C$ with $b = 0$, from eq 19 as observed in Figure 7 ($I_e \sim C^{1.5}$).

For perylene, using $\tau_m = 5.8$ ns and $k = 8 \times 10^6$ (mM)⁻¹(s)⁻¹ from literature⁷ and $a(\lambda_{ex} = 408 \text{ nm}) = 4.30$ (mM)⁻¹(mm)⁻¹ from the experiment, $a(\lambda_{ex} = 532 \text{ nm})$ is adjusted to obtain $a(\lambda_{ex} = 532 \text{ nm}) = 4.0 \times 10^{-5}$ (mM)⁻¹(mm)⁻¹. With these parameters, $I_m \cong I_e$ if $C = (1/\tau_m k) = 21.6$ mM on resonant excitation. In the experiment, the condition of $C < 21.6$ mM is satisfied in the whole range of the measured concentration, so that $I_m > I_e$ from eqs 13 and 14. This explains the difficulty in observing excimer emission on resonant excitation. The resonant excimer emission is expected to be included in the low energy tail (1.8 to 1.9 eV) of the resonant monomer emission spectrum as in Figure 3. The integrated photon flux density in this energy region is plotted with open squares in Figure 8. The fitting curve is obtained as the weighted sum of the resonant monomer and excimer emission photon flux densities using the experimentally determined ratios ($P_m = 0.00285$ and $P_e = 0.147$) of the photon flux density in this energy region against the whole monomer (low- C) and excimer emission spectra. Agreement is fairly good considering that only two fitting parameters are used in this analysis. For nonresonant excimer emission (only E-emission is fitted), the experimental result shows the linear dependence on C , while the present model tells that the linear dependence should appear for the higher C . This fact indicates that the model needs further refinement.

V. DISCUSSION

The concentration dependence of the nonresonant excimer emission in pyrene is explained nearly perfectly by the simple model based on the ordinary excimer formation process considering collision between the excited and ground-state monomer molecules: first an isolated molecule is excited to the excited state, then the excited molecule interacts with one of the surrounding ground-state molecules. But the excimer generation efficiency, which is represented by the fitting parameter $a(\lambda_{ex,nonresonant})$, looks extraordinarily high as explained in the following.

If excimers are formed via the ordinary process, the final state by nonresonant photoexcitation should be located above the minimum point of the excited-state adiabatic potential. In this case the initial state should be thermally populated levels in the ground-state adiabatic potential as shown in Figure 9. The thermal population is evaluated by the Boltzmann factor $\exp(-\Delta E/k_B T)$, where ΔE is detuning of the excitation energy from the 0–0 transition energy, k_B is the Boltzmann constant, and T is temperature. The relative population of the thermally populated state with respect to the zero-phonon state is evaluated to be 2.4×10^{-5} , 5.9×10^{-9} for detuning corresponding to 488 nm, 532 nm in perylene, 6.2×10^{-7} for 408 nm in pyrene (For pyrene, 3.4 eV is taken as the 0–0 transition for the ¹L_b state. Considering the oscillator strength is $\sim 1/100$ compared with the resonant excitation band, it should be further 1/100 times smaller). The ratio of photon flux density of the nonresonantly excited excimer emission to the resonantly excited monomer emission is expected to be as small as this value. However, the experimental results in Figures 7 and 8 show a much higher ratio by more than 2 orders of magnitude larger than these estimates. This suggests that there is a more efficient excitation mechanism for excimer formation.

If nonresonant excitation occurs from thermally populated levels in the electronic ground state to the zero-phonon state in the electronically excited state, anti-Stokes luminescence should be observed to the same relative amount as in the resonant

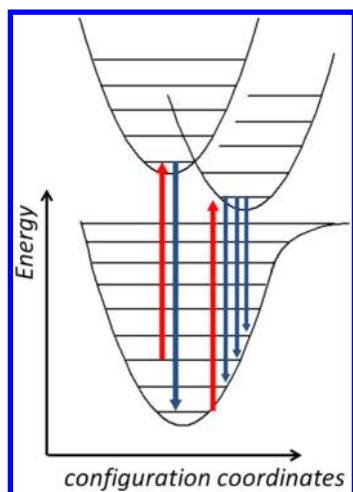


Figure 9. Nonresonant excitation in molecules from thermally populated excited vibrational levels, resulting in anti-Stokes emission. Nonresonant excitation in nanocrystals, which resonantly excites excimers from the zero-phonon state, resulting in the absence of anti-Stokes emission.

excitation case, as shown in Figure 9. In fact, there are significant anti-Stokes components in the nonresonant excimer emission spectra for perylene solution in Figure 3. By contrast, it is striking that anti-Stokes components are almost absent for nonresonant excimer emission in perylene nanocrystals in Figure 4. This strongly suggests that excimers in nanocrystals are resonantly excited directly from the bottom in the ground state as depicted in Figure 9. This is considered to be due to a symmetry-breaking effect close to the surface of nanocrystals.²⁰ A similar trend is also observed in the high-concentration PMMA samples as in Figure 5, where the reabsorption effect is negligibly small.

These observations lead to a possible excimer formation mechanism in solution schematically depicted in Figure 10. The excited molecule interacts with a ground-state molecule to form an excimer.^{5,6} The intermolecular coordinates for excimer formation are multidimensional including parallel displacement and molecular rotation. The figure just highlights a typical

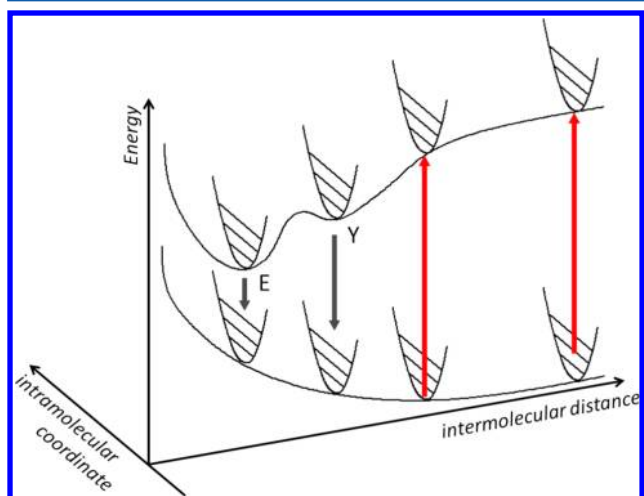


Figure 10. Potential energy of ground and excited states as a function of intermolecular and intramolecular coordinates. There are two types of nonresonant excitation (red upward arrows of the same length) leading to excimer formation.

excimer formation path as the intermolecular distance. Intramolecular coordinates are represented by the orthogonal axis against the intermolecular axis. The double minima in the excited-state intermolecular adiabatic potential correspond to the E and Y states for the case of perylene. In this model, nonresonant excitation below the 0–0 transition energy of an isolated molecule is enabled as resonant 0–0 excitation along the intermolecular excimer formation path as weakly interacting molecules. This excitation may lead to Y- or E-emission as the molecules approach each other along the path, or anti-Stokes emission as the molecules deviate from the path. The population of nonisolated (interacting) molecules may be higher than that of thermally vibrationally excited molecules, and a symmetry-broken intermolecular configuration relaxes a degree of the forbidden transition compared to ideally arranged excimers as observed in nanocrystals. These two effects are a possible mechanism of efficient excimer formation on nonresonant excitation.

There is a possibility that molecules are excited at the long tail of the homogeneously broadened absorption. There is no report about the phase relaxation time T_2 of pyrene and perylene in solution. It is reasonable to adopt $T_2 = 100$ fs for both pyrene and perylene in solution, since a dye molecule in solution at room temperature is reported to have $T_2 \sim 50$ fs, although it is uncertain whether the zero-phonon line is studied or not.²¹ Then, the ratio of the absorption strength of the tail to the peak is estimated to be 7.6×10^{-5} for pyrene (tail at 3.04 eV, peak at 3.7 eV), 4.8×10^{-4} and 1.5×10^{-4} for perylene (tail at 2.54 and 2.33 eV, peak at 2.82 eV) using the Lorentz model. For both pyrene and perylene, these ratios are rather close to the observed ratios of the photon flux density of nonresonant excimer emission to resonant monomer emission in Figures 7 and 8. However, this estimation gives the photon flux density of almost the same order of magnitude in Y- and E-emission for perylene (only 3 times difference) because the Lorentzian has a long tail, while in the experiment there is a 100 times difference in the photon flux density between Y- and E-emission.

There remains a possibility of the contribution of impurities for excimer(-like) emissions in perylene solution. The E-emission intensity is smaller by 5 to 6 orders of magnitude than the monomer emission intensity, so that a ppm order of impurities can not be neglected. Pentacene has almost the same melting point as perylene, so that there is possible contamination with pentacene. Monomer emission of pentacene is definitely discriminated from the observed E-emission, but oxidized products of pentacene such as pentaquinone may have a similar broad structureless emission in the same energy region.²² In addition, oxidized products such as perylene quinone²³ are also possible impurities. Presently, the possibility of such a contribution can not be ruled out, but the close resemblance of nonresonant emission spectra among solutions, polymer films, and nanocrystals in Figure 4 supports excimer formation in solution. In addition, as in Figure 9, the emitted photon flux density decreases by 2 orders of magnitude as the detuning is increased by 0.21 eV from 2.54 eV (488 nm) to 2.33 eV (532 nm) excitation. This fact is more consistent with excimer emission than two kinds of impurities being included at this ratio accidentally.

Another possibility is a contribution of molecular aggregates, i.e., nanocrystals or clusters, formed even in unsaturated solution due to the dynamic equilibrium between monomers and aggregates. The contribution from nanocrystals as large as 100 nm can be excluded because they show nonresonant

behavior as in Figure 4 characterized by the absence of Y-emission. Since the behavior for much smaller aggregates is unknown, a trace amount of such molecular aggregates may contribute to nonresonant excimer emission. This picture is not far from the model in Figure 10. They are continuously connected to each other. At least, we can not detect any appreciable change in the spectral shapes of emission and absorption as a function of the concentration, except for features already known for dimer formation in the absorption spectra (Supporting Information).²⁴

VI. CONCLUSION

It is found that excimer emission in pyrene and perylene in solution is exclusively observed using nonresonant one-photon excitation with cw lasers below the monomer absorption edge. The concentration dependence of the excimer emission intensity suggests that the ordinary excimer formation process from excited- and ground-state molecules is important, but the excimer formation efficiency is extraordinarily high considering the detuning of the excitation energy from the monomer resonance. In order to identify the excimer formation mechanism on nonresonant excitation, a further investigation is needed taking into account such a contribution as resonant excitation of loosely interacting dimers or as molecular aggregates formed in the balance of dynamical equilibrium.

■ ASSOCIATED CONTENT

Supporting Information

The effect of dissolved oxygen on photoluminescence intensity and decay time of pyrene in ethanol solution, detailed examination of crystal formation in perylene/PMMA films by measuring space-resolved extinction spectra, and comparison of luminescence and absorption spectral shapes for the concentration range studied are given in Figures S1–S7. This information is available free of charge via the Internet at <http://pubs.acs.org>.

■ AUTHOR INFORMATION

Corresponding Author

*Electronic address: eiji@rs.kagu.tus.ac.jp.

Notes

The authors declare no competing financial interest.

■ ACKNOWLEDGMENTS

The authors thanks Mr. Yoshinao Okuda and Mr. Takumi Isono for their assistance in measuring time-resolved luminescence and space-resolved extinction spectra, respectively, in the Supporting Information.

■ REFERENCES

- (1) Tanaka, J. The Electronic Spectra of Aromatic Molecular Crystals. II. The Crystal Structure and Spectra of Perylene. *Bull. Chem. Soc. Jpn.* **1963**, *36*, 1237–1249.
- (2) Nishimura, H.; Yamaoka, T.; Mizuno, K.; Iemura, M.; Matsui, A. Luminescence of Free and Self-Trapped Excitons in α - and β -Perylene Crystals. *J. Phys. Soc. Jpn.* **1984**, *53*, 3999–4008.
- (3) Birks, J. B.; Dyson, D. J.; Munro, I. H. 'Excimer' Fluorescence. II. Lifetime Studies of Pyrene Solutions. *Proc. R. Soc. London A* **1963**, *275*, 575–588.
- (4) Birks, J. B.; Lumb, M. D.; Munro, I. H. 'Excimer' Fluorescence. V. Influence of Solvent Viscosity and Temperature. *Proc. R. Soc. London A* **1964**, *280*, 289–297.

- (5) Winnik, F. M. Photophysics of Preassociated Pyrenes in Aqueous Polymer Solutions and in Other Organized Media. *Chem. Rev.* **1993**, *93*, 587–614.

- (6) Birks, J. B.; Christophorou, L. G. 'Excimer' Fluorescence. IV. Solution Spectra of Polycyclic Hydrocarbons. *Proc. R. Soc. London A* **1964**, *277*, 571–582.

- (7) Katoh, R.; Sinha, S.; Murata, S.; Tachiya, M. Origin of the stabilization energy of perylene excimer as studied by fluorescence and near-IR transient absorption spectroscopy. *J. Photochem. Photobiol. A: Chem.* **2001**, *145*, 23–34.

- (8) Johnson, P. C.; Offen, H. W. Perylene Excimer Fluorescence in Cyclohexane. *Chem. Phys. Lett.* **1973**, *18*, 258–260.

- (9) Walker, B.; Port, H.; Wolf, H. C. The Two-Step Excimer Formation in Perylene Crystals. *Chem. Phys.* **1985**, *92*, 177–185.

- (10) Sumi, H. Two Kinds of Excimers in α -Perylene and Pyrene Crystals: Origin of Y and V Emissions. *Chem. Phys.* **1989**, *130*, 433–449.

- (11) Fujiwara, H.; Kawazoe, T.; Ohtsu, M. Nonadiabatic Multi-Step Excitation for the Blue-Green Light Emission from Dye Grains Induced by the Near-Infrared Optical Near-Field. *Appl. Phys. B: Laser Opt.* **2010**, *98*, 283–289.

- (12) Le, T. H. H.; Mawatari, K.; Pihosh, Y.; Kawazoe, T.; Yatsui, T.; Ohtsu, M.; Tosa, M.; Kitamori, T. Optical Near-Field Induced Visible Response Photoelectrochemical Water Splitting on Nanorod TiO₂. *Appl. Phys. Lett.* **2011**, *99*, 213105 1–3.

- (13) Ujjiye-Ishii, K.; Kwon, E.; Kasai, H.; Nakanishi, H.; Oikawa, H. Methodological Features of the Emulsion and Reprecipitation Methods for Organic Nanocrystal Fabrication. *Cryst. Growth Des.* **2008**, *8*, 369–371.

- (14) Ishino, H.; Iwai, S.; Iwamoto, S.; Okumura, T.; Nishimoto, T.; Nair, S. V.; Kobayashi, T.; Tokunaga, E. Absorption and Emission Spectra of Molecular Excitons in Single Perylene Nanocrystals. *Phys. Rev. B* **2011**, *84*, 041303(R) 1–4.

- (15) Williams, R. Observation of the Relative Polarizations of Electronic Transitions. *J. Chem. Phys.* **1957**, *26*, 1186–1188.

- (16) Parker, C. A.; Hatchard, C. G. Delayed Fluorescence of Pyrene in Ethanol. *Trans. Faraday Soc.* **1963**, *59*, 284–295.

- (17) Ham, N. S.; Ruedenberg, K. Electronic Interaction in the Free-Electron Network Model for Conjugated Systems. II. Spectra of Aromatic Hydrocarbons. *J. Chem. Phys.* **1956**, *25*, 13–26.

- (18) Ferreira, J. A.; Porter, G. Concentration Quenching and Excimer Formation by Perylene in Rigid Solutions. *J. Chem. Soc., Faraday Trans. 2* **1977**, *73*, 340–348.

- (19) Salamon, Z.; Bassler, H. Fluorescence Properties of Perylene Aggregates in a Polymer Matrix (PMMA). *Chem. Phys.* **1985**, *100*, 393–400.

- (20) Fujino, T.; Tahara, T. Femtosecond Fluorescence Up-Conversion Microscopy: Exciton Dynamics in α -Perylene Microcrystal. *J. Phys. Chem. B* **2003**, *107*, 5120–5122.

- (21) Moshary, F.; Arend, M.; Friedberg, R.; Hartmann, S. R. Ultrafast Relaxation and Modulation in the Oxazine Dye Nile Blue. *Phys. Rev. A* **1992**, *46*, R33–36.

- (22) Bhalla, V.; Roopa; Gupta, A.; Dhir, A.; Kumar, M. A Pentaquinone-Based 4–2 Bit Photonic Encoder. *Dalton Trans.* **2011**, *40*, 5176–5179.

- (23) Chowdhury, P. K.; Dasa, K.; Datta, A.; Liu, W.-Z.; Zhang, H.-Y.; Petrich, J. W. A Comparison of the Excited-State Processes of Nearly Symmetrical Perylene Quinones: Hypocrellin A and Hypomycin B. *J. Photochem. Photobiol. A: Chem.* **2002**, *154*, 107–116.

- (24) Ferguson, J. Absorption and Emission Spectra of the Perylene Dimer. *J. Chem. Phys.* **1966**, *44*, 2677–2683.